Use of Wigner-Ville transformations for fluid particles in laser Doppler flow accelerometry [†]

Sejong Chun[*] and Hyu-Sang Kwon[*]

Division of Physical Metrology, Korea Research Institute of Standards and Science, Daejeon, 305-340, Korea

---

Abstract

Flow acceleration with Lagrangian description is crucial to understanding particle movements in turbulent jet flows or dissipation statistics in isotropic turbulence. Laser Doppler anemometry is regarded as a suitable experimental tool for measuring flow acceleration, because scattering particles generate trajectories in the measurement volume, which process gives rise to flow acceleration at a fixed measuring point with the Lagrangian description. The most useful algorithm for processing Doppler signals is either the quadrature demodulation technique (QDT) or the iterative parametric method (alternatively, the minimization of least squares, LSM) as in the literature. In the present study, another algorithm using the Wigner-Ville transform (W-V) is introduced to give more accurate estimation of flow acceleration than the QDT or the LSM. Five signal-processing algorithms, including the QDT, the LSM, the MC (maximization of correlation), and the W-V, were compared with each other in experiments with an impinging air jet flow with a cylindrical rod and a round free-air jet flow. Mean flow acceleration distribution in the streamwise direction was mainly investigated. Processing speeds for the above-mentioned signal-processing algorithms were checked to find the best algorithm, which has best performance with short processing time. Although QDT was found to be an accurate algorithm with short processing time, it has limited applications to flows with large acceleration and high SNR. The MC was also found to be a good algorithm with moderate processing speed, which can be useful in flows with low SNR because the MC is an iterative parametric method. The W-V gave the most accurate values for flow acceleration; however, the processing time for this method was the slowest among the signal-processing algorithms.

Keywords: Lagrangian description; Laser Doppler accelerometry; Metrology; Signal processing; Uncertainty analysis

---

1. Introduction

Flow acceleration with Lagrangian description is crucial to understanding particle movements in turbulent jet flows or dissipation statistics in isotropic turbulence [1, 2]. Non-invasive optical techniques, such as the laser Doppler anemometry (LDA), the particle tracking velocimetry (PTV) and the particle image velocimetry (PIV), can provide measurement of flow acceleration as well as of flow velocity [1, 3, 4]. All these techniques measure flow velocity at fixed points, which represent the Eulerian description of fluid flows. However, in the case of LDA, flow acceleration can be obtained with the Lagrangian description, even though the measurement location is fixed at the coordinates according to the Eulerian description. It is because the measurement volume, in which two laser beams intersect, is large enough for scattering particles to undergo changes of flow velocity, when they pass through the fringes in the measurement volume. Because burst

signals record particle trajectories in terms of phase, the LDA can obtain flow acceleration by revealing the phase information in the burst signals. Second-order differentiation of the phase in the burst signals can give flow acceleration, which is Lagrangian [5-9]. This is called laser Doppler accelerometry.

For processing burst signals by the LDA, Lehmann et al. (2002) have developed most of the signal processing algorithms [4]. These algorithms are classified into three types: non-parametric (2-pt FFT), direct-parametric, and iterative-parametric (alternatively, the minimization of least squares, LSM) algorithms. Nobach et al. (2006, 2010) and Nobach (2008) developed another signal processing algorithm, which exploits an iterative-parametric method, namely, the maximization of correlation (MC) to reduce processing time for estimating flow acceleration with the same accuracy, as that of the LSM [5-7]. Bayer et al. (2008) preferred to adopt the quadrature demodulation technique (QDT) with narrow band-pass filtering in developing a laser Doppler profile sensor [8].

However, there has yet been no mention of the time-frequency technique, such as the use of Wigner-Ville transforms (W-V). When Gazengel and Poggi (2005) measured acoustic particle velocities in an enclosed sound field, they

---

used the time-frequency technique [10]. There is also a controversial issue that the time-frequency algorithm, such as the short time Fourier transforms (STFT) and the W-V, might have an averaging effect that gives an offset from the averaged flow acceleration [8].

In the present study, an LDA with a fiber-optic probe is employed to measure flow acceleration with the Lagrangian description in an impinging jet flow with a circular cylinder and a round free-air jet flow. Streamwise distribution of flow acceleration is measured along both the main flow direction and the radial direction, in the case of the round free-air jet flow. Derived flow acceleration, namely, $\frac{VdV}{dx}$, plays a role as a reference value to test the measured flow accelerations, which are derived from the five signal processing algorithms (the 2pt-FFT, the QDT, the LSM, the MC, and the W-V). The processing time of each signal processing algorithm is also checked to consider calculation efficiency in obtaining the flow accelerations.

2. Experimental apparatus and methods

2.1 A fiber-optic LDA system

A commercial 2-component fiber-optic LDA system (IFA 750, TSI Inc.) was used to measure flow velocity and flow acceleration in 1) an impinging jet flow with a circular cylinder and 2) a round free-air jet flow; the apparatuses are shown in the schematic diagram (Figs. 1 and 2). A 3 W Ar$^+$ laser (Inova 70C, Coherent Inc.) generated a laser beam to the LDA. A multicolor beam separator (Color Burst 9201, TSI Inc.) divided the laser beam into three wavelengths: 476.0, 488.0 and 514.5 nm. The Bragg cell in the multicolor beam separator induced frequency shifts to the laser beams to differentiate the laser beams into unshifted and shifted components. RF signals with 40 MHz from a multicolor receiver (Color Link 9230, TSI Inc.) were induced to operate the Bragg cell. Two wavelengths of the laser beams, namely, (488.0 and 514.5) nm components, consisted of each velocity component in a fiber-optic LDA probe.

For the fiber-optic LDA probe, the focal length of the transmitting lens was 362.8 mm, and the diameter of the lens was 60 mm. The cross angles between the two laser beams were 7.88° at 488.0 nm, and 7.89° at 514.5 nm. The expanded uncertainty for the beam crossing angle was found to be less than 0.22 % (k = 2.26). The averaged values of fringe spacing were 3.55 μm at 488.0 nm, and 3.74 μm at 514.5 nm. Commercial software (FIND, TSI Inc.) was used to define hardware settings for the signal processor (IFA 750). The FIND software was used to control the PMT (photo multiplier tube) voltage within (770 ~ 920) V, the band pass frequency of (0.3 ~ 3) MHz at (2 ~ 10) m/s and (1 ~ 10) MHz at (10 ~ 30) m/s, and the shift frequency at 200 kHz during the measurement of burst signals.

An in-house program with LabVIEW (8.6.1, NI Inc.) defined the sampling frequency of 100 MHz, the high-pass cut-
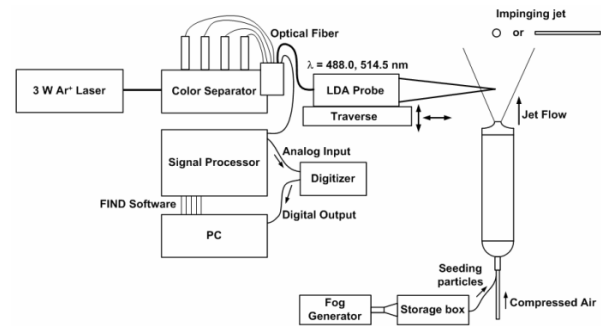

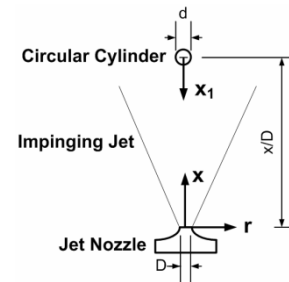Fig. 1. Schematic diagram of measuring flow acceleration with LDA.

Fig. 2. Schematic diagram of an impinging jet with a circular cylinder.

off frequency of 3 MHz, the input voltage range of 2 V$_{pk-pk}$ and the trigger level of ±0.02 V. An 8-bit digitizer (USB-5133, NI Inc.) sampled burst signals via the signal processor, as indicated in Fig. 1. The number of measurements for burst signals was 1,000 in the present experiment. MATLAB (7.10, Mathworks Inc.) was used to implement a narrow-band signal filtering and the five signal processing algorithms-the 2-pt FFT, the QDT, the LSM, the MC and the W-V-to calculate the flow velocity and the flow acceleration with the burst signals [4-10].

2.2 Alignment of a LDA probe

A laser beam profiler (BeamON-VIS, Duma Optronics Inc., Israel) was used to measure the distribution of light intensity in the cross section of the laser beams. The CCD sensor of the laser beam profiler identified the crossing point of the two laser beams. Both the unshifted and the shifted beams showed good correlation with the Gaussian distribution at the cross section. The unshifted beams at 488.0 and 514.5 nm showed correlation values with the Gaussian distribution of more than 90 %, while the shifted beams at 488.0 and 514.5 nm had correlation values of more than 88.5%.

For detailed diagnosis of the laser beams, the beam quality factor M^2, which identifies the beam waist diameter, should have been measured [11]. Because M^2 is the ratio between the beam parameter product of a laser beam and that of an ideal Gaussian beam at the same wavelength, the Gaussian beam has the lowest possible beam parameter product [11]. However, M^2 has not been measured due to limitations of

the present apparatus. Another type of beam profiler with a rotating slit, combined with an automated traverse, would be desirable for diagnosis of M^2. Instead, beam diameters of laser beams were measured by installing a pinhole with diameter of 20 μm (P20S, Thorlabs Inc.) in front of a laser power meter (1918-C, 918D-SL-OD3, Newport Inc.). The beam diameters were 0.15 mm when the output power of the Ar^+ laser was less than 1 W.

A microscope lens was located at the focal plane of the transmitting lens, which was attached on the LDA probe. The purpose of the microscope lens was to locate the beam crossing point at the focal plane of the transmitting lens. The laser beams were aligned by projecting them through the microscope lens on the wall. The laser beam at wavelength of 476 nm was also projected through the receiving optics to indicate the correct position for beam alignment. Three images by projecting the laser beams were coincident on the wall. The projected images were focused on a point by adjusting the tilting angles of two collimators, which were attached in the rear part of the LDA probe [12].

Variation of fringe spacing was measured with a rotating wheel by traversing the LDA probe in the horizontal direction, because the variation of fringe spacing affected the accuracy of flow acceleration as well as flow velocity. In addition, large portions of the expanded uncertainty for flow velocity measurement by the LDA came from the fringe divergence in the measurement volume [13-15]. The validation rate was defined as the normalized sampling time to collect a certain number of burst signals, e.g., 5,000 samples, divided by the total sampling time. The validation rate could be regarded as a probability density function to limit the effective range of burst signals in the measurement volume. It was because most of the burst signals were recorded when the scattering particles passed through the central area of the measurement volume. The distribution of the validation rate exhibited a shape similar to that of the Gaussian distribution because the number of samples was large enough to satisfy the central limit theorem [16]. The validation rate indicated that meaningful burst signals were found at -0.5 mm < z < 0.5 mm. Here, z was the horizontal axis of the measurement volume centered at the crossing point of the two laser beams. The expanded uncertainty for the fringe spacing was found to be within 0.49 % ($k = 2.20$) at 488.0 nm, and 0.48 % ($k = 2.18$) at 514.5 nm.

2.3 Principle of LDA and its signal processing algorithms

A burst signal can be defined as a sinusoidal function with a Gaussian window, and the argument of the sinusoidal function possesses information on flow velocity and flow acceleration [4, 8, 16].

$$s(t) = e^{-\eta t^2} cos\left(\frac{\pi A}{\Delta x}t^2 + \frac{2\pi V}{\Delta x}t + \phi_0\right) \tag{1}$$

Here, $s(t)$ is a burst signal, A is the flow acceleration

[m/s²], V is the flow velocity [m/s], η is a constant to determine the width of the Gaussian window [1/s²] which has a typical value of 3.125, ϕ_0 is phase angle [rad], t is time [s], and Δx is the fringe spacing in the measurement volume [μm]. Δx is denoted as follows:

$$\Delta x = \frac{\lambda}{2sin(\theta/2)}. \tag{2}$$

Here, λ is the wavelength of two laser beams [nm], θ is the crossing angle of the two laser beams [rad]. In the present study, Δx = 3.55 μm (488.0 nm) or 3.74 μm (514.5 nm) as described in the section 2.1.

Doppler frequency f_D can be expressed as in the following [16]:

$$f_D = \frac{V}{\Delta x} = \frac{2Vsin(\theta/2)}{\lambda}. \tag{3}$$

In most cases, f_D can be obtained from the burst signal by assuming that there is no flow acceleration ($A = 0$). In this case, f_D can be identified as the dominant frequency calculated by Fourier transforms of $s(t)$. If A is to be calculated, more elaborate signal processing algorithms other than the Fast Fourier Transform (FFT) must be introduced.

The first method to calculate A can be the 2-pt FFT. In this method, a burst signal is normalized to one by dividing the signal amplitude of the burst signal with the amplitude imposed by the Gaussian window. The normalized signal is then divided into two halves. Two separate Gaussian windows are multiplied to the first and the second fraction of the burst signal, respectively. If two f_D are calculated by applying Eq. (3) for each fragment of the burst signal, both V and A can be obtained as follows [4]:

$$V = \frac{f_D(t)+f_D(t+\Delta t)}{2}\Delta x, \tag{4}$$

$$A = \frac{f_D(t+\Delta t)-f_D(t)}{\Delta t}\Delta x. \tag{5}$$

Here, Δt is the time difference of two central points between the first and the second fraction of the burst signal. If the signal length of $s(t)$ is T and the length of each fragmented signals is $\frac{T}{2}$, Δt can be $\frac{T}{2}$. Δt can be changed by a careful selection considering how to divide the signal $s(t)$ [4]. The 2-pt FFT algorithm can also be referred to as a nonparametric algorithm in the literature [4].

The second method to calculate A is the quadrature demodulation technique (QDT). The QDT is a direct method to induce A by unwrapping the phase in the sinusoidal function of Eq. (1) [4, 8]. Sometimes, the Hilbert transform is used to unwrap the phase of a burst signal, which consists of complex variables. It is because the burst signal can be implemented by using a digital down-conversion (DDC) technique [8, 16]. The

QDT provides an unbiased estimator for V and A [4, 8]. However, the QDT is susceptible to electrical noises of the burst signal [4]. Therefore, a bandpass filtering is necessary to increase the signal-to-noise ratio (SNR) in evaluating V and A calculated by the QDT [8]. If unwrapped phase is denoted by ϕ, the unwrapped phase is expressed as in the following equation:

$$\phi = tan^{-1}\left(\frac{\tilde{s}(t)}{s(t)}\right). \qquad (6)$$

Here, $s(t)$ is the Hilbert transform of $s(t)$. To induce V and A, a second-order curve fitting is applied to the un-wrapped phase [4, 8].

The third method to calculate A is the minimization of least square method (LSM) using an optimization algorithm. In the literature, the LSM is categorized into an iterative parametric algorithm [4]. Eq. (1) becomes a model equation describing the burst signal measured by the LDA. The Least square sum, e, between the measured burst signal and the modeled burst signal is calculated as in the following:

$$e = \sum\left(\hat{s}(t) - s(t)\right)^2. \qquad (7)$$

Here, $\hat{s}(t)$ is the modeled burst signal according to Eq. (1) and $s(t)$ is the measured burst signal. V, A and $\hat{\phi}_0$ of $\hat{s}(t)$ can be thought of as the best estimate of V and A, if the first-order partial differentiations of e with respect to V, A and $\hat{\phi}_0$ are equal to zero to minimize e. A MATLAB function (fminunc) facilitates this calculation to find V, A and $\hat{\phi}_0$ [17, 18].

The fourth method to calculate A is the maximization of correlation (MC) using the same optimization algorithm. The main difference between the MC and the LSM is how to construct the least square sum [5-7].

$$e = -\sum \hat{s}(t)s(t) \qquad (8)$$

In this case, ϕ_0 of $\hat{s}(t)$, derived from Eq. (1), becomes useless, because the correlation of two signals is only important. Therefore, the modeled burst signal $\hat{s}(t)$ can have two unknown parameters V and A. This reduces some complexities in calculating the two parameters with the same MATLAB function (fminunc).

Finally, the fifth method to calculate A is to use the Wigner-Ville transform (W-V). The W-V considers $s(t)$ as a function of both time and frequency by linearly chirping the signal [19, 20].

$$W_s(t,f) = \int_{-\infty}^{\infty} s(t+\tau/2)s^*(t-\tau/2)e^{-j2\pi f\tau}d\tau \qquad (9)$$

Here, $W_s(t,f)$ is the Wigner-Ville transform, τ is time delay [s], f is frequency [Hz], and $s^*(t)$ is the complex conjugate of $s(t)$. A MATLAB function (tfrwv) is used to
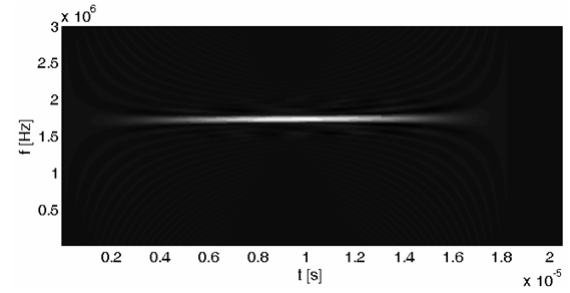
(a) Wigner-Ville transforms
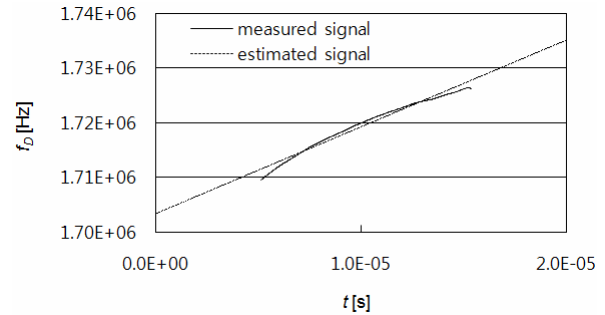
(b) Variations of Doppler frequency

Fig. 3. Signal processing of a burst signal using the Wigner-Ville transforms.

calculate the Wigner-Ville transform [19]. To induce V and A, a first-order curve fitting is applied to the ridge of iso-contours of the W-V as seen in Fig. 3.

2.4 Uncertainty analysis of flow velocity and acceleration

Standard uncertainty of V can be derived as follows, referring to the ISO guide [21]:

$$u(V) = \left(\left(\frac{\partial V}{\partial \lambda}u(\lambda)\right)^2 + \left(\frac{\partial V}{\partial \theta}u(\theta)\right)^2 + \left(\frac{\partial V}{\partial f_D}u(f_D)\right)^2\right)^{0.5} \qquad (10)$$

Here, $u(V)$ is the standard uncertainty of V [m/s], $u(\lambda)$ is the standard uncertainty of λ [nm], $u(\theta)$ is the standard uncertainty of θ [rad], and $u(f_D)$ is the standard uncertainty of f_D [Hz]. $u(\lambda)$ and $u(\theta)$ are the type B uncertainties, which have some fixed values. On the contrary, $u(f_D)$ becomes the type A uncertainty, which can have different values depending on the signal processing algorithms [21]. If the expanded uncertainty, $U(V) = ku(V)$, is calculated, it has values less than 0.55 % (k = 2.09) at 488.0 nm, and 0.48 % (k = 2.11) at 514.5 nm. The expanded uncertainty is displayed as error bars in the subsequent figures (Figs. 4(a)-7(a)), and the uncertainty levels are comparable to those found in the literature on the uncertainty analysis of LDA [13-15, 22].

To estimate the standard uncertainty of A, Eq. (3) is differentiated with respect to time as in the following equation:

$$A = \frac{DV}{Dt} = \frac{\lambda}{2sin(\theta/2)} \frac{Df_D}{Dt}. \tag{11}$$

Even though Eq. (11) is plausible in principle, there are some difficulties in estimating $\frac{Df_D}{Dt}$, because the material derivative of f_D must be determined experimentally. This explains why various signal processing algorithms are existing to obtain V and A from $s(t)$. An alternative method to derive the standard uncertainty of A is to assume the steady state of flow conditions during measurement of the burst signals. This enables to consider only the convective term in the material derivative of V with respect to t.

$$A = \frac{DV}{Dt} \sim V\frac{dV}{dx} = \frac{\lambda^2 f_D}{4sin^2(\theta/2)} \frac{df_D}{dx} \tag{12}$$

Here, $\frac{df_D}{dx}$ is the spatial derivative of f_D in the main flow direction across the LDA measurement volume [1/m·s]. The standard uncertainty of A can be expressed as in the following equation:

$$u(A) = \left(\begin{array}{c} \left(\left(\frac{\partial A}{\partial \lambda}u(\lambda)\right)^2 + \left(\frac{\partial A}{\partial \theta}u(\theta)\right)^2 + \left(\frac{\partial A}{\partial f_D}u(f_D)\right)^2 \right) \\ + \left(\frac{\partial A}{\partial \left(\frac{df_D}{dx}\right)}u\left(\frac{df_D}{dx}\right)\right)^2 \end{array} \right)^{0.5} \tag{13}$$

Here, $u(A)$ is the standard uncertainty of A [m/s^2], and $u\left(\frac{df_D}{dx}\right)$ is the standard uncertainty of $\frac{df_D}{dx}$ [1/m·s]. $u\left(\frac{df_D}{dx}\right)$ is the type A uncertainty, which has two main uncertainty factors. One is related to random errors in measuring random fluctuations of fluid particles by turbulent flows. The other is related to fringe divergence in the LDA measurement volume [4-8]. Although the flow acceleration fluctuations can be incorporated into estimating the random errors, the effect of fringe divergence cannot be estimated until analytical expressions to describe the fringe spacing in the LDA measurement volume are identified [11, 23]. It is because the description on the fringe spacing includes the identification of the beam waist location, as mentioned in the section 2.2. The error bars to indicate the measurement ranges of A in the subsequent figures (Figs. 4(c)-7(e)) are based on the expanded uncertainty of A, $U(A) = ku(A)$, which might be underestimating $u\left(\frac{df_D}{dx}\right)$ due to the difficulty in determining the beam waist locations.

2.5 Apparatus for generating jet flow

A cylindrical apparatus was used to generate jet flows by injecting compressed air, as shown in Fig. 1 [24]. Three perforated plates were installed in the apparatus to stabilize the compressed air flow. A regulator (AR4000-04, SMC Inc.) was used to control the inlet pressure at around 0.3 bar. Another regulator of the same type (AR4000-04) confined the flow rates of the compressed air to (619 ~ 736) L/min. The compressed air was emitted to the atmosphere as exhaust through a nozzle attached to the apparatus. A fog generator (F2010, SAFEX Inc.) generated scattering particles by heating fog fluids (Blitz Reflex, SAFEX Inc.). The fog fluids were used according to the manufacturer's instructions to produce scattering particles with an average diameter of 1.55 μm with a poly-disperse distribution of (0.05 ~ 2.85) μm [25]. There were slight co-flows for seeding the particles, because there was a connecting tube between the storage box of the fog generator and the cylindrical apparatus, as shown in Fig. 1. There should be little influence of the co-flows to the velocity distribution in the jet flows, because the co-flows were generated by pressure difference between the storage box and the cylindrical apparatus.

An ISA nozzle with diameter of 25 mm was attached to the apparatus to generate a round free-air jet flow. The flow velocity and the flow acceleration distributions were measured between 10 mm and 390 mm from the nozzle exit plane in the streamwise direction. Radial distributions of the streamwise flow velocity and the streamwise flow acceleration were also measured at (10, 150 and 300) mm from the nozzle exit plane. During the jet flow measurements, the ambient temperature was (23.0 ± 0.6) °C (k = 2). The atmospheric pressure was maintained at (1.008 ± 0.002) bar (k = 2), and the relative humidity was (51.5 ± 0.7) % (k = 2).

A 3-axis traverse (VP 9000, Velmex Inc.) was used to locate the measurement volume of the LDA in the jet flows. This enabled precise measurements of the flow velocity and flow acceleration in the streamwise direction along the center line of the nozzle and in the radial direction. In the case of measuring the radial distribution of the streamwise flow velocity component, the measurement volume was moved in a direction perpendicular to the laser beam axis. This removed the ambiguity that arose by the fact that the measurement volume axis was aligned to the radial direction.

In the round free-air jet, two flow conditions (Q = 619 L/min and 736 L/min) were specified by flow velocity at the nozzle exit plane. The nozzle exit velocity was different for the different flow conditions, e.g., 21 m/s at Q = 619 L/min and 25 m/s at Q = 736 L/min. The potential core of the jet flows was identified within $\overline{D}$ = 5, where D was the nozzle diameter. The Reynolds number was in the range of 33,000 ~ 39,000 for the round free-air jet.

Geometrical parameters, illustrated in Fig. 2, describe flow configurations for an impinging jet flow with a cylindrical rod. The circular cylinder with diameter of 15 mm turned the round free-air jet into the impinging jet. The flow velocity and the flow acceleration were measured in a range between 1 mm and 10 mm from the surface of the circular cylinder. In the impinging jet flow, the Reynolds number based on the nozzle diameter was 39,000.

3. Experimental results and discussion
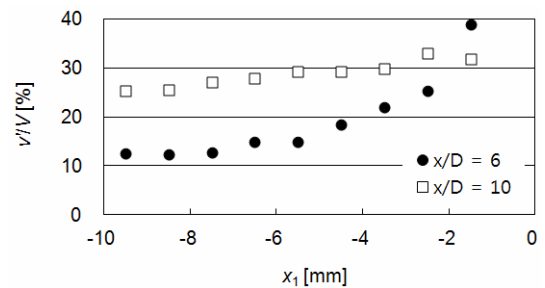
3.1 An impinging jet with a circular cylinder

An impinging jet was generated by placing a circular cylinder in a round free-air jet flow, as shown in Figs. 1 and 2, to examine the measurement accuracy of the flow acceleration [8]. The impinging jet imparted large decelerations to the scattering particles in the vicinity of the cylinder, as displayed in Fig. 4(a). In the figure, x_1 is defined as the horizontal axis from the center of the cylinder against the flow direction (see Fig. 2). The measurement location was confined to -10 mm $\leq$ $x_1 \leq -1$ mm. The cylinder was located at $\overline{D}$ = 6 or 10 from the jet exit plane. The SNR of burst signals in the flow was 20.7 ± 0.2 dB in the vicinity of the cylinder.

When the cylinder was located at $\frac{x}{D}$ = 6, the mean velocity decreased as x_1 approached to -1 mm. Turbulence intensity increased due to the large velocity fluctuations stemming from the impingement of flow on the cylinder surface. The amount of velocity change was reduced at $\frac{x}{D}$ = 10 because the cylinder was located further downstream compared with the case of $\frac{x}{D}$ = 6. The increase of turbulence intensity at $\frac{x}{D}$ = 10 was also smaller than that of $\frac{x}{D}$ = 6. Mean flow accelerations at both $\frac{x}{D}$ = 6 and 10 exhibited deceleration in the range of (-30,000 ~ 0) m/s^2, as shown in Figs. 4(c) and 4(d). Flow deceleration at $\frac{x}{D}$ = 6 was larger than that at $\frac{x}{D}$ = 10, because there were stronger velocity changes in the vicinity of the cylinder. The error bars are also shown in the figures and the range of deviation can be seen to be on the order of O (1,000 m/s^2).

The derived flow acceleration is denoted in Fig. 4 as $\frac{VdV}{dx}$. Because the derived acceleration was based on the flow velocity, the magnitude of the error bars was rather smaller than that of measured flow acceleration by various signal processing algorithms. Therefore, $\frac{VdV}{dx}$ could be used as the reference value to examine the accuracy of the various signal processing algorithms [4]. However, the derived flow acceleration was only applicable in the flows, where velocity gradients could be measured, such as the impinging jet. The measured and the derived flow accelerations displayed good agreement, as can be seen in Figs. 4(c) and 4(d), because there were strong flow decelerations in the impinging jet. Flow decelerations at $\frac{x}{D}$ = 10 showed better agreement than those at $\frac{x}{D}$ = 6. This discrepancy might be because the accuracy of flow deceleration measurement was dependent on the magnitude of the flow acceleration as well as on the relative fluctuations of the acceleration, $\frac{a'}{A}$. About this, it could be conjectured that the turbulence intensity might give an idea of the measurement accuracy of the flow acceleration. For example, in a flow with higher turbulence intensity, the relative acceleration fluc-
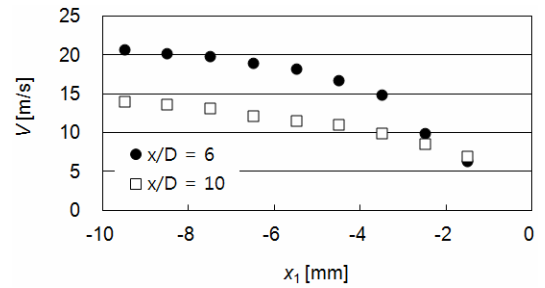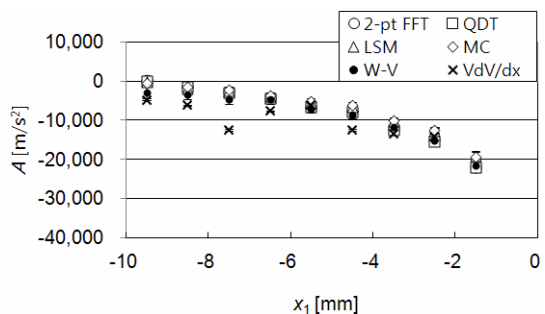

(a) Mean velocity

(b) Turbulence intensity
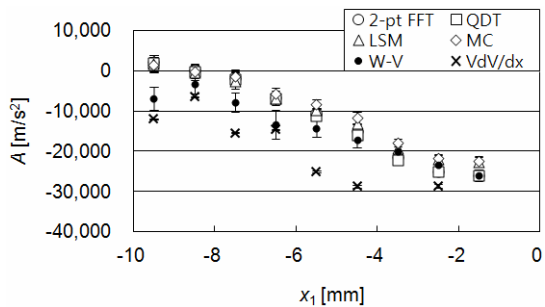
(c) Mean acceleration at $x/D = 6$

(d) Mean acceleration at $x/D = 10$

Fig. 4. Flow velocity and flow acceleration in an impinging jet with a circular cylinder.

tuations $\frac{a'}{A}$ were large enough to reduce the lowest possible limit for flow acceleration. Therefore, the different turbulence levels agreed better between the measured and the derived flow accelerations at $\frac{x}{D}$ = 10. In particular, the W-V agreed with the derived flow acceleration better than other signal-processing algorithms. The agreement is prominent where

both the turbulence intensity and the mean flow acceleration is low, at $x_1 \leq -6$ mm and $\frac{x}{D} = 6$.

Bayer et al. (2008) showed the measured flow acceleration distribution around a thin metal wire in a uniform flow [8]. The measurement location was -0.2 mm $\leq x_1 \leq 0.05$ mm and the diameter of the metal wire was 80 μm. The flow deceleration was measured at -1,200,000 m/s^2 $\leq A \leq 0$ m/s^2. Therefore, the flow deceleration was very large and the extent of the measurement location was very small compared with the present experimental setup. This was possible because the laser Doppler profile sensor measured the flow acceleration distribution within three overlaps of measurement volume [8]. Therefore, the laser Doppler profile sensor could provide high SNR of burst signals, which induced quite good agreements between the measured and the derived flow accelerations in the vicinity of the wire. On the contrary, the present LDA setup could measure only one flow acceleration value within the measurement volume. This imposed spatial limitations on the flow acceleration measurement in the impinging jet flow with the circular cylinder. For example, the flow deceleration was (-30,000 ~ 0) m/s^2 in the range of -10 mm $\leq x_1 \leq$ -1 mm, as shown in Figs. 4(c) and 4(d). The minimum measurable flow acceleration was lowered and the measurement locations for flow acceleration were extended in comparison to those values shown in the previous work [8].

In addition, the location of the circular cylinder ($\frac{x}{D} = 6$ and 10) was not in the potential core region but in the turbulent flow region of the round free-air jet. The location of the circular cylinder affected the quality of agreement between the measured and the derived flow accelerations in terms of the SNR of burst signals and the turbulence intensity. This was because the SNR of the burst signals and the turbulence intensity decreased as the measurement location went upstream from the surface of the circular cylinder.

3.2 A round free-air jet: streamwise distribution of streamwise flow velocity and acceleration

A round free-air jet was generated to further examine the performance of flow acceleration measurement by the signal processing algorithms. The inlet streamwise velocities were (21 and 25) m/s, which corresponded to Q = (619 and 736) L/min, respectively. Here, Q is the flow rate discharged from the nozzle. The inlet streamwise velocities were measured at $\frac{x}{D} = 0.4$ because of the limited accessibility of the LDA probe in the vicinity of the nozzle in the jet flow. The SNR was 17.0 ± 0.2 dB at $\frac{x}{D} = 10$, when Q = 736 L/min; therefore, the SNR was lower than the SNR in the impinging jet flow.

The mean velocity distributions indicate that the measurement range of 0 $\leq \frac{x}{D} \leq 5$ belonged to the potential core, as can be seen in Fig. 5(a). The mean velocity distribution was relatively constant in this region. As flow went downstream

(a) Mean velocity

(b) Turbulence intensity

(c) Acceleration at $Q = 619$ L / min

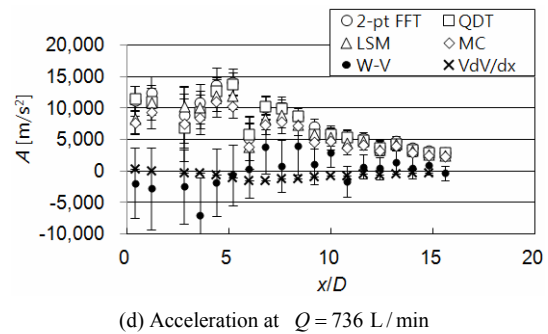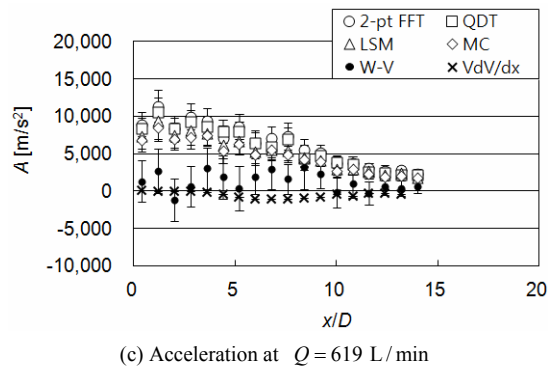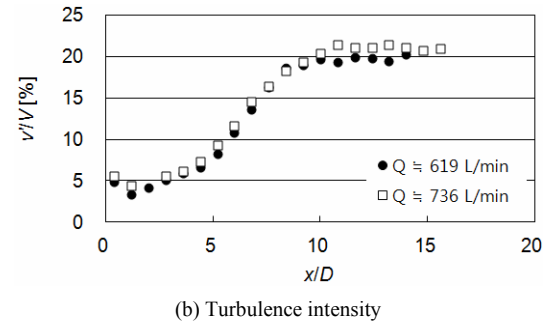(d) Acceleration at $Q = 736$ L / min
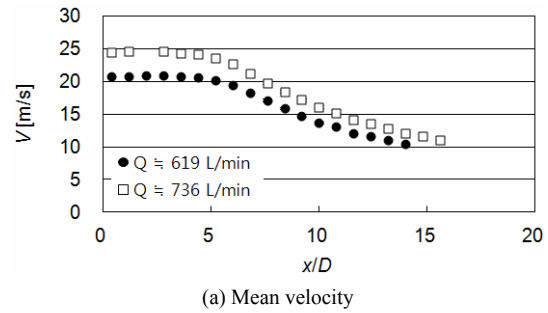
Fig. 5. Flow velocity and flow acceleration in a round free-air jet (streamwise direction).

from $\frac{x}{D} = 5$, the mean velocity decreased. The flow velocity distribution did not show any self-similarity because the self-similarity region began at $\frac{x}{D} > 30$, while the measurement range was less than $\frac{x}{D} = 15$ [26]. The turbulence intensity in the potential core was about 5 %. The turbulence intensity increased, when the measurement location went downstream

from $\dfrac{x}{D}$ = 5 to 10, as can be seen in Fig. 5(b). After that, the turbulence intensity attained at around 20 % at $\dfrac{x}{D}$ > 10. The turbulence intensity levels between the two flow rates of Q = (619 and 736) L/min were almost identical.

The derived flow acceleration gave rather weak flow decelerations in the jet flow because there were no means of flow impingement like a circular cylinder, which can generate strong velocity decelerations in the streamwise direction. The derived flow acceleration was -1,000 m/s$^2 \leq$ A $\leq$ 120 m/s^2 at Q = 619 L/min, and -1,500 m/s$^2 \leq$ A $\leq$ 300 m/s^2 at Q = 736 L/min, as found in Figs. 5(c) and 5(d). The signal-processing algorithms, except for the W-V, produced flow accelerations greater than zero (1,700 m/s$^2 \leq$ A $\leq$ 11,500 m/s^2). However, the W-V estimated flow accelerations at around zero flow acceleration between (-7,000 and 4,000) m/s^2, with relatively large error bars. Because of these error bars, it seemed that W-V might give correct values for flow acceleration, which was consistent with the derived flow acceleration.

3.3 A round free-air jet: radial distribution of streamwise flow velocity and acceleration

Radial distributions of streamwise flow velocity and acceleration were displayed when Q = 619 L/min, as shown in Fig. 6. The measurement locations were $\dfrac{x}{D}$ = 0.4, 6 and 12. The mean velocity distribution showed the effect of mixing as the measurement locations went downstream of the nozzle, as shown in Fig. 6(a). The turbulence intensity distribution indicates the effect of mixing at the shear layers where the jet and the quiescent flow met [26]. The turbulence intensity amounted to 30 % of the mean flow velocity, as indicated in Fig. 6(b). Note that error bars for V are hidden behind each symbol except at $\dfrac{x}{D}$ = 12 in Fig. 6(a). This means that $u(V)$ is small, except for the region where turbulence levels are greater than 20 %, as seen in Fig. 6(b).

The measured flow accelerations between the W-V and the other signal-processing algorithms did not agree with each other, as can be seen in Figs. 6(c)~6(e). The W-V showed flow accelerations within (-2,000 ~ 2,400) m/s^2 at $\dfrac{x}{D}$ = 0.4, while the other signal-processing algorithms displayed rates between -2,800 m/s^2 and 8,200 m/s^2, as can be seen in Fig. 6(c). In comparison with the streamwise distribution of the derived flow accelerations $\dfrac{VdV}{dx}$ seen in Fig. 5(c), the W-V might give a better distribution of flow accelerations in the radial direction.

At $\dfrac{x}{D}$ = 6, there were also discrepancies of flow accelerations between the W-V and the other signal-processing algorithms in Fig. 6(d). The discrepancy was clearly observed
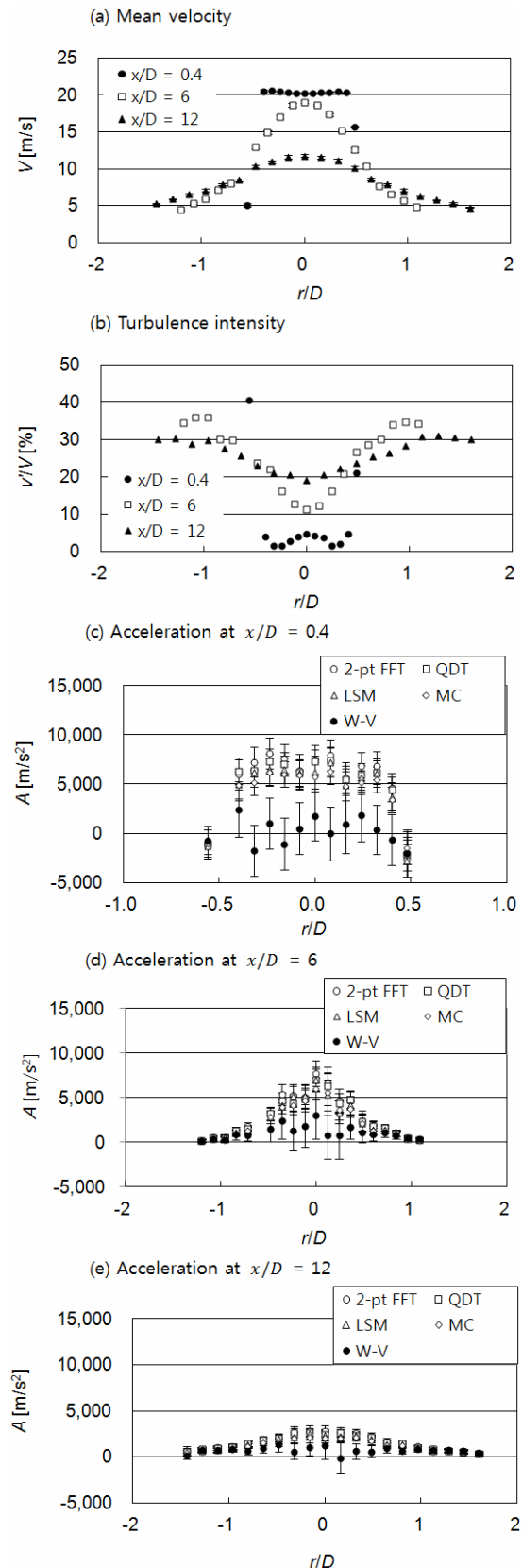

Fig. 6. Flow velocity and flow acceleration in a round free-air jet at Q = 619 L/min (radial direction).
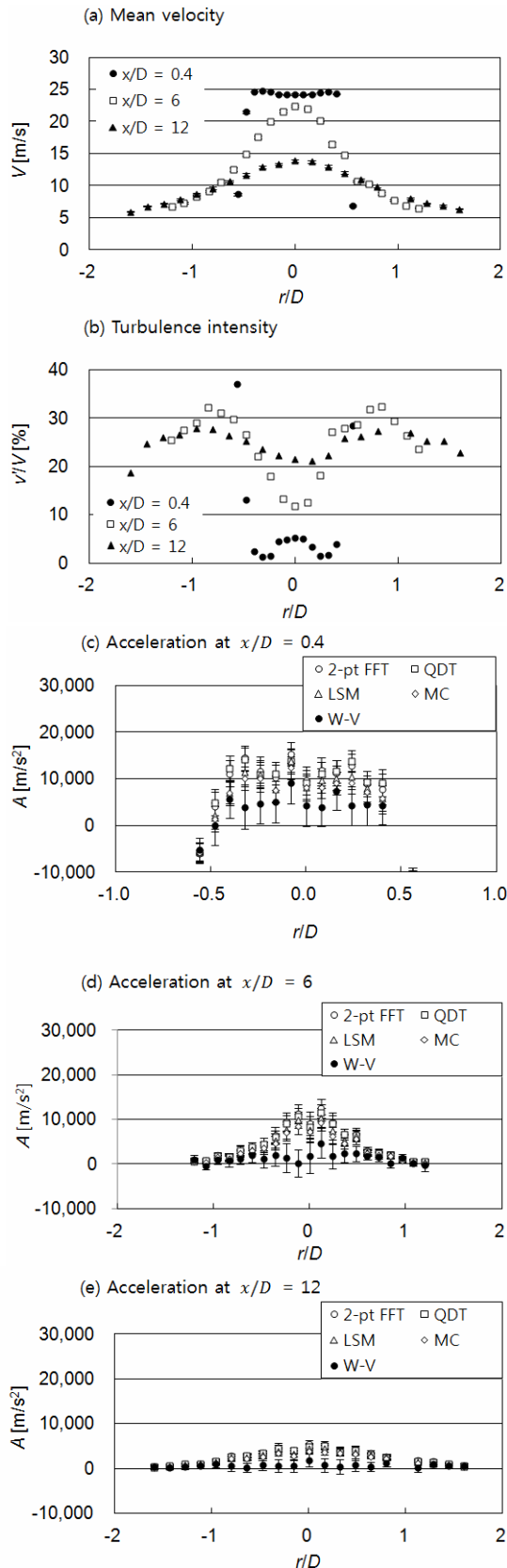
Fig. 7. Flow velocity and flow acceleration in a round free-air jet at $Q = 736$ L/min (radial direction).

Table 1. Processing speed of the signal processing algorithms.

cpu time	Impinging jet with circular cylinder		Impinging jet with flat plate		Round free-air jet	
[ms]	$x/D = 6$	$x/D = 10$	$x/D = 2$	$x/D = 10$	$V_0 = 21$ m/s (619 L/min)	$V_0 = 25$ m/s (736 L/min)
FFT	1.14	1.34	1.38	1.27	1.61	1.58
2pt-FFT	1.34	1.48	1.62	1.41	1.74	1.61
QDT	2.62	3.02	3.18	2.86	3.60	3.50
LSM	299.89	333.60	365.68	294.50	362.69	347.27
MC	142.80	155.52	127.97	104.75	127.90	119.91
W-V	694.14	955.60	695.66	895.93	891.79	824.00

when $-0.5 < \dfrac{r}{D} < 0.5$. However, the discrepancy seemed to be reduced as the measurement location was moved farther away from the center of the jet ($\dfrac{r}{D} < -0.5$ or $\dfrac{r}{D} > 0.5$). This might also be explained in relation to the turbulence intensity levels. For example, at $-0.5 < \dfrac{r}{D} < 0.5$ and $\dfrac{x}{D} = 6$, the turbulence intensity was less than 27%. At $\dfrac{r}{D} < -0.5$ or $\dfrac{r}{D} > 0.5$, the lowest possible flow acceleration should be reduced to less than 15,000 m/s^2. This means that the accuracy of the flow accelerations was dependent on the lower limit of the flow acceleration, which was incurred by the turbulence intensity levels. This tendency also applied to the case with $\dfrac{x}{D} = 12$, shown in Fig. 6(e). In this case, the region where all the signal-processing algorithms agreed was expanded toward the central area in the jet flow, because the overall turbulence intensity increased more than 20%, for the entire region of jet flow.

The same explanation could be extended to the radial distribution of streamwise flow velocity and acceleration when $Q = 736$ L/min, as shown in Fig. 7. The only difference was that the mean flow acceleration increased to twice the original value in comparison with the case of $Q = 619$ L/min.

3.4 Processing speed of signal-processing algorithms

The processing speeds of the signal processing algorithms for estimating flow velocity and flow acceleration are summarized in Table 1. The processing speeds indicate the elapsed CPU time, which is taken to obtain the flow velocity and the flow acceleration, independent of the operating systems. From the data in Table 1, cost-effective algorithms could be found. For example, the FFT was the fastest algorithm, because it calculated flow velocity without estimating flow acceleration. The 2-pt FFT followed the FFT, because the 2-pt FFT calculated both flow velocity and acceleration using the FFT algo-

rithm. The QDT was also a fast algorithm, and was comparable in processing speed to the 2-pt FFT. The QDT might be one of the most cost-efficient algorithms, because it showed good agreement with the derived acceleration ($\frac{VdV}{dx}$) in the impinging jet with the circular cylinder, as indicated in Fig. 4. However, in the round free-air jet flow, the QDT did not agree well with the derived acceleration, as shown in Fig. 5. Therefore, the performance of the QDT in measuring the flow acceleration depended on the flow configurations, such as the high SNR and the low turbulence intensity.

The LSM and the MC must be robust algorithms, because these algorithms are derived from iterative parametric methods, which optimize flow parameters of a burst signal by iteration [5-7]. The two algorithms gave similar estimations for flow acceleration in both the impinging jet and the round free-air jet. In terms of the processing speed, the MC was two times faster than the LSM, as indicated in Table 1. Therefore, the MC was more cost-effective than the LSM, when one of the two iterative algorithms had to be chosen for flow acceleration measurement.

The W-V showed similar measurement accuracy for flow acceleration in comparison with the QDT in the impinging jet with the circular cylinder, as is shown in Fig. 4. The processing speed of the W-V was the slowest among the signal-processing algorithms, taking more than twice the time of the LSM. However, considering the good agreement with the derived flow accelerations in the impinging jet and the round free-air jet, the W-V provided the closest estimate values of the flow acceleration for the derived flow acceleration. Therefore, the W-V showed not only the best accuracy but also the slowest processing speed in the measurement of flow acceleration.

4. Conclusions

Flow acceleration with the Lagrangian description is crucial to understanding particle movements in turbulent jet flows or dissipation statistics in isotropic turbulence. A fiber-optic LDA system was used to measure the flow acceleration in an impinging jet flow with a circular cylinder and a round free-air jet flow. The expanded uncertainty of the flow velocity with the LDA was within 0.55% (k = 2.09) at 488.0 nm, and 0.48 % (k = 2.11) at 514.5 nm, which values were comparable to those of previous studies. In the flow experiments with impinging jets and a round free-air jet, the turbulence intensity levels played an important role in agreements between the measured and the derived flow accelerations. High turbulence intensity with SNR more than 20.7 ± 0.2 dB was important for obtaining correct values of flow acceleration. The processing speed of the five signal processing algorithms was examined (the 2pt-FFT, the QDT, the LSM, the MC, and the W-V). The QDT was considered to be accurate with high processing speed; however, the QDT was only applicable to flows with large deceleration and high SNR more than 20.7 dB. The MC was regarded as a good algorithm with moderate processing

speed, because it is applicable to burst signals with SNR as low as 17.0 dB. The W-V gave the most accurate value for flow acceleration, comparable to derived flow acceleration. The W-V was applicable to burst signals with relatively low SNR of 17.0 dB. However, the processing speed was the slowest among the signal-processing algorithms. Therefore, it was found that the W-V is a useful algorithm for flow accelerometry, although the W-V takes a great deal of processing time for analysis.

Nomenclature————————————————————

A	: Flow acceleration [m/s^2]
$\widehat{A}$	: Estimated value of flow acceleration [m/s^2]
D	: Nozzle diameter [mm]
Q	: Flow rate [L/min]
$U(A)$	: Expanded uncertainty of A [m/s^2]
$U(V)$	: Expanded uncertainty of V [m/s^2]
V	: Flow velocity [m/s]
$\widehat{V}$	: Estimated value of flow velocity [m/s]
W_s	: Wigner-Ville transforms of $s(t)$
a'	: Standard deviation of A [m/s^2]
e	: Least square sum [V^2]
f	: Frequency [Hz]
f_D	: Doppler frequency [Hz]
k	: Coverage factor
r	: Radial direction [mm]
$s(t)$	: Burst signal [V]
$s^*(t)$	: Complex conjugate of $s(t)$ [V]
$\tilde{s}(t)$	: Hilbert transforms of $s(t)$ [V]
$\hat{s}(t)$	: Modeled burst signal of $s(t)$ [V]
t	: Time [s]
$u(A)$	: Standard uncertainty of A [m/s^2]
$u(V)$	: Standard uncertainty of V [m/s]
$u\left(\frac{df_D}{dx}\right)$	: Standard uncertainty of $\frac{df_D}{dx}$ [mm]
$u(f_D)$	: Standard uncertainty of f_D [Hz]
$u(\Delta t)$	: Standard uncertainty of Δt [s]
$u(\theta)$	: Standard uncertainty of θ [rad]
$u(\lambda)$	: Standard uncertainty of λ [nm]
v'	: Standard deviation of V [m/s]
x	: Main flow direction [mm]
x_1	: Horizontal axis from the center of an object [mm]
Δt	: Time difference [s]
Δx	: Fringe spacing [μm]
η	: Constant to characterize the Gaussian window [1/s^2]
θ	: Beam crossing angle [rad]
λ	: Wavelength of laser beam [nm]
τ	: Time delay [s]
ϕ_0	: Phase angle [rad]
$\widehat{\phi}_0$	: Estimated value of phase angle [rad]

References

[1] A. L. Porta, G. A. Voth, A. M. Crawford, J. Alexander and E. Bodenschatz, Fluid particle accelerations in fully developed turbulence, *Nature*, 409 (2001) 1017-1019.

[2] P. K. Yeung, S. B. Pope, A. G. Lamorgese and D. A. Donzis, Acceleration and dissipation statistics of numerically simulated isotropic turbulence, *Physics of fluids*, 18 (6) (2006) 065103-1.

[3] K. T. Christensen and R. J. Adrian, Measurement of instantaneous acceleration fields using particle-image velocimetry, *4th International Symposium on Particle Image Velocimetry* (*PIV '01*), September 17-19, Göttingen, Germany (2001) Paper 1080.

[4] B. Lehmann, H. Nobach and C. Tropea, Measurement of acceleration using the laser Doppler technique, *Measurement Science and Technology*, 13 (2002) 1367-1381.

[5] H. Nobach, M. Kinzel and C. Tropea, Measurement of Lagrangian acceleration in turbulent flows using the laser Doppler technique, *Proceedings of SPIE*, 6262 (2006) doi:10.1117/12.682916 http://dx.doi.org/10.1117/12.682916.

[6] H. Nobach, Messung von Teilchenbeschleunigungen mit dem Laser-Doppler-Anemometer, *AHMT Symposium*, September 11-13, Dresden, Germany (2008).

[7] H. Nobach, M. Kinzel, R. Zimmermann, C. Tropea and E. Bodenschatz, Measurement of particle accelerations with the laser Doppler technique, *Notes on Numerical Fluid Mechanics*, 110 (2010) 271-278.

[8] C. Bayer, K. Shirai, L. Büttner and J. Czarske, Measurement of acceleration and velocity components using a laser Doppler velocity profile sensor, *Measurement Science and Technology*, 19 (2008) 1-11.

[9] K. T. Lowe and R. L. Simpson, Measurements of velocity-acceleration statistics in turbulent boundary layers, *International Journal of Heat and Fluid Flow*, 27 (2006) 558-565.

[10] B. Gazengel and S. Poggi, Measurement of acoustic particle velocities in enclosed sound field: Assessment of two laser Doppler velocity measuring systems, *Applied Acoustics*, 66 (2005) 15-44.

[11] A. E. Siegman, How to (maybe) measure laser beam quality, *Tutorial presentation at the Optical Society of America Annual Meeting*, October, Long Beach, California, USA (1997)(http://www.stanford.edu/~siegman/beams_and_resonators /beam_quality_tutorial_osa.pdf).

[12] TSI Incorporated, *Single-component fiber-optic probe system: instruction manual*, St. Paul, Minnesota, USA (1990).

[13] T. T. Yeh and J. M. Hall, Uncertainty of NIST airspeed calibrations, *Measurement Science Conference*, March 10-14, Anaheim, California, USA (2008).

[14] N. Kurihara, Y. Terao and M. Takamoto, LDV calibrator for the air speed standard between 1.3 to 40 m/s, *5th International Symposium on Fluid Flow Measurement*, April 8-10, Arlington, Virginia, USA (2002).

[15] C. –T. Yang, M. –C. Wu and H. –S. Chuang, Adjustment and evaluations of an LDA probe for accurate flow measurement, *Optics and Lasers in Engineering*, 38 (2002) 291-304.

[16] H. –E. Albrecht, N. Damaschke, M. Borys and C. Tropea, *Laser Doppler and phase Doppler measurement techniques*, Springer, Heidelberg, Germany (2003).

[17] MathWorks, *Optimization Toolbox 5: User's Guide*, Natick, MA, USA (2010) 146-161.

[18] MathWorks, *Signal Processing Toolbox 6: User's Guide*, Natick, MA, USA (2010) 923- 924.

[19] F. Auger, P. Flandrin, P. Goncalves and O. Lemoine, *Time-frequency toolbox: for use with MATLAB*, CNRS(France) and Rice University (USA) (1996).

[20] L. Debnath, *Wavelet transforms and their applications*, Springer, Heidelberg, Germany (2002).

[21] International Standard Organization, *Uncertainty of measurement, Part 3: Guide to the expression of uncertainty in measurement* (*GUM:1995*), ISO/IEC Guide 98-3:2008, Geneva, Swiss (2008).

[22] F. Durst, R. Müller and A. Naqwi, Measurement accuracy of semiconductor LDA systems, *Experiments in Fluids*, 10 (1990) 125-137.

[23] P. C. Miles, Geometry of the fringe field formed in the intersection of two Gaussian beams, *Applied optics*, 35 (30) (1996) 5887-5895.

[24] S. Chun, S. H. Lee and Y. M. Choi, Calibration system for three-cup anemometers, *Transactions of the KSME B*, 34 (3) (2010) 325-331 (in Korean).

[25] Dantec Dynamics, *SAFEX fog generator user's guide*, September 24, no. 40U5971, Skovlunde, Denmark (2003).

[26] S. B. Pope, *Turbulent flow*, Cambridge University Press, Cambridge, United Kingdom (2000) 96-103.

Sejong Chun is a research engineer working at KRISS in Korea. He joined the Division of Physical Metrology since 2004. He majored in fluid mechanics for his Ph.D study under Professor Hyung Jin Sung's supervision at KAIST in Korea. He also visited Professor Cam Tropea's laboratory at TU Darmstadt in Germany for one year after his graduation. His research interests are the liquid flow rate metrology, the ultrasound flow tomography and the fluid acceleration using LDA.

Hyu-Sang Kwon is a Principal Research Scientist working at KRISS in Korea. He joined the Division of Physical Metrology since 1998. He majored in acoustics for his Ph.D. study under Professor Yang-Hann Kim's supervision at KAIST in Korea. He also visited Herrick laboratory in Purdue University for one year after his graduation. His major research interests include acoustic array techniques used in air, underwater, and structure as well as acoustic measurement and testing techniques.